

RSC Advances



This is an *Accepted Manuscript*, which has been through the Royal Society of Chemistry peer review process and has been accepted for publication.

Accepted Manuscripts are published online shortly after acceptance, before technical editing, formatting and proof reading. Using this free service, authors can make their results available to the community, in citable form, before we publish the edited article. This *Accepted Manuscript* will be replaced by the edited, formatted and paginated article as soon as this is available.

You can find more information about *Accepted Manuscripts* in the [Information for Authors](#).

Please note that technical editing may introduce minor changes to the text and/or graphics, which may alter content. The journal's standard [Terms & Conditions](#) and the [Ethical guidelines](#) still apply. In no event shall the Royal Society of Chemistry be held responsible for any errors or omissions in this *Accepted Manuscript* or any consequences arising from the use of any information it contains.

Polysiloxane-Functionalized Graphene Oxide Paper: Pyrolysis and Performance as Li-ion Battery and Supercapacitor Electrode

M. S. Kolathodi^{†*a}, L. David^{†a}, M. A. Abass^a and G. Singh^{*a}

^a Mechanical and Nuclear Engineering Department, Kansas State University, Manhattan, Kansas, 66506, United States

*E-mail: muhamed@ksu.edu, Tel.: +1-785-317-4325

gurpreet@ksu.edu, Tel.: +1-785-532-7085. Fax: +1-785-532-7057

ABSTRACT

Exfoliated graphene oxide (GO) and polysiloxane were blended and pyrolyzed to synthesize free-standing SiOC-graphene composite papers. Characterization techniques reveal a layer-by-layer stacking of GO sheets and an increase in interlayer spacing due to the functionalization of SiOC with GO. This unique structure of the SiOC-graphene composite paper makes it suitable for energy storage application in batteries and supercapacitors. A reversible electrochemical capacity $\sim 750 \text{ mAh g}^{-1}$ which stabilized to $\sim 400 \text{ mAh g}^{-1}$ after 5 cycles was recorded when tested as a battery electrode. Also, a maximum specific capacitance of 75.72 F g^{-1} at a current density of 6.7 A g^{-1} was observed while studying its electrochemical performance as a supercapacitor.

1. INTRODUCTION

Electrochemistry-based energy storage systems have been the focus of intense research in today's energy driven community.^{1,2} In this context, research into energy storage devices such as batteries (e.g. lithium-ion (LIBs) and sodium-ion (SIBs) batteries) and supercapacitors have shown to satisfy important requirements like energy density and high power density with excellent performance during cycling.³⁻⁶ Electrode materials like graphene oxide-based composites have received much attention recently due to their improved electrical conduction, flexibility, lightness and high performance in rechargeable energy storage devices.⁷⁻²⁴ However, there are major challenges that have to be resolved before they can be considered as an attractive alternative to existing electrode materials. For example, in batteries, the cyclability of these electrodes is limited by the amount of lithium (Li) or sodium (Na) active phase that the paper can bear, which generally varies from 50 to 70%.⁶ Furthermore, the active material is decorated on the surfaces of graphene rather than being accommodated between the individual graphene sheets, making them vulnerable to being peeled off upon continuous ion insertion and extraction.²⁵⁻³⁰ In addition, these inclusion particles may not be evenly dispersed in the electrode, leading to aggregation, which in turn could lead to an increase in the electronic path length resulting in poor rate capability.³¹

One alternative to improving the electrochemical performance and mechanical flexibility of graphene-based electrodes is by fabricating a sandwich structure of graphene composite in which the active material forms a thin intimate coating on either side of the graphene layer.³² To this end, active materials based on molecular precursor-derived ceramics (PDCs) such as silicon oxycarbide (SiOC) – also referred to as polysiloxane – have been developed. The formation of a simultaneous bond between Si, O and C atoms makes it different from other Si-based electrode materials.³³ In battery anodes, the presence of a SiOC active phase in a porous and amorphous network can offer certain advantages in terms of processing and Li-cyclability, which includes:

- 1) PDCs being derived from thermal decomposition of liquid polymeric precursors were proven to interface with carbonation materials like graphite and carbon nanotubes (CNTs) in the liquid phase.³⁴⁻³⁸
- 2) Because of their disordered carbon structure, these glass-ceramics are predicted to form a path of least resistance for ionic diffusion and electron conduction, thereby offering improved C-rate performance.³⁹⁻⁴²
- 3) The PDC structure is generally rigid and chemically stable, which would cause the electrode to maintain intimate contact during lithiation/delithiation processes.^{24,34,42}
- 4) Dangling bonds of Si and C act as Li intercalation sites and improve reversible charge capacity.⁴³
- 5) Open and porous structure of PDCs aids in increased electrochemical performance even at very high current densities.⁴⁴⁻⁴⁹

The possibility of tailoring the properties of SiOC ceramic composites by using different precursors makes them one of the choicest materials for electrochemical energy storage. The composites are commonly synthesized via pyrolytic conversion of a liquid polymer to a solid ceramic. Depending on the conversion process, different ceramic morphology such as powders,^{50,51} paper films⁶ and fibers⁵² have been reported. Kim et al. have reported the synthesis of SiOC from poly(phenyl carbosilane). The powdered SiOC were made into LIB electrodes by producing them in a slurry (containing PVDF and binder) on a copper foil and later dried. The supported electrode showed a stable charge capacity of 360 mAh g⁻¹ at a current density of 0.2 mA cm⁻² after 9 cycles.⁵³ In another study, Singh et al. prepared a shell-core SiOC-CNT composite via controlled pyrolysis of a SiOC precursor (tetravinyl cyclotetrasiloxane, TTCS) and CNT. Improved charge capacity and cycling stability compared to the neat SiOC and CNT electrodes were reported.³⁴ The SiOC battery electrodes reported in aforementioned studies were made from slurry containing some additives namely: polymer solvent, binder and conducting agent. The addition of these additives increases the production cost of these

electrodes and possibly dampens the desirable electrochemical properties of the active material. For instance, it is well known that the porous structures of composites could be clogged by the presence of binders. Also, side reaction of the electrode and electrolyte with the polymer solvent and the binder could occur, thereby degrading the performance of the cell.⁵² In addition, the presence of additives and the use of a metal support (e.g. copper foil) contributes to dead weight of the electrode material, which is undesirable for lightweight electrochemical energy storage applications.

In this paper, we demonstrated the synthesis of a ceramic/reduced GO sandwich paper by intercalating liquid TTCS between individual GO sheets during a layer-by-layer vacuum filtration assembly process. Upon pyrolysis, the intercalated TTCS oligomers were transformed to SiOC ceramic and simultaneously, GO was reduced to reduced graphene oxide (rGO), forming a layer-by-layer SiOC-rGO composite (LBL-SiOC-rGO). The sandwich structure not only guarantees solid contact between the SiOC molecules and the graphene layer, it also facilitates high electrode conductivity, renders the elastomeric space needed to accommodate the volume changes associated with Li-cycling (thus leading to improved performance as battery electrodes) and also provides the required surface area for the interaction of the electrolyte with LBL-SiOC-rGO. Furthermore, we compared the performance of the as-synthesized LBL-SiOC-rGO paper with pyrolyzed polyvinyl alcohol on GO (PVA-rGO) paper electrode (prepared under similar conditions) and demonstrate that the improvement in Li-cyclability and capacity value is not only due to the open structure of the paper and that SiOC thin layers trapped between the graphene layers are critical to achieving high Li-charge capacity. In addition, we evaluated the electrochemical performance of LBL-SiOC-rGO as a supercapacitor by comparing it with PVA-rGO and pyrolyzed poly (methyl methacrylate) on GO (PMMA-rGO) prepared with a procedure similar to PVA-rGO.

2. EXPERIMENTAL SECTION

2.1 Materials

Sodium nitrate (NaNO_3 , 99.2%), potassium permanganate (KMnO_4 , 99.4%), sulfuric acid (H_2SO_4 , 96.4%), hydrogen peroxide (H_2O_2 , 31.3% solution in water), hydrochloric acid (HCl , 30% solution in water), and ethanol ($\text{C}_2\text{H}_5\text{OH}$, 99.9%) were purchased from Fisher Scientific. Polyvinyl alcohol (PVA) and poly (methyl methacrylate) (PMMA) were purchased from Alfa Aesar. All materials were used as received without further purification.

2.2 Preparation graphene oxide

Modified Hummer's method was used to make graphene oxide.^{54,55} Concentrated H_2SO_4 (130 mL) was added to a mixture of graphite flakes (3 g, Sigma Aldrich) and NaNO_3 (1.5 g). The mixture was cooled down using an ice bath. KMnO_4 was added slowly to this mixture. The mixture was stirred for 12 h at 50 °C. Then, it was quenched with water (400 mL) and 30% H_2O_2 (3 mL) while in an ice bath such that the temperature did not exceed 20 °C. The remaining material was washed in succession with 200 mL of water twice, 200 mL of 30% HCl and 200 mL of $\text{C}_2\text{H}_5\text{OH}$. The remaining material after these extended washes was filtered through a paper filter. The filtrate was dried overnight to obtain dry graphene oxide (GO).

2.3 Preparation of reduced graphene oxide and LBL-SiOC-rGO, PVA-rGO and PMMA-rGO composite papers

10 mL colloidal suspension of GO in 1:1 (v/v) water was made by sonication for 10 minutes. To this solution, tetravinyl cyclotetrasiloxane (TTCS, Gelest, PA) consisting of 10 wt.% dicumyl peroxide (Sigma Aldrich) – a crosslinking agent - in 10 mL of isopropanol (ISP) (Fisher Scientific) was added and the mixture was further sonicated for 60 minutes and stirred for 6 h. Once the composite suspension was made, it was filtered by vacuum filtration through a 10 μm filter membrane (HPLC grade, Millipore). The LBL-TTCS-GO composite paper obtained was carefully

removed from the filter paper and dried. PVA-rGO and PMMA-rGO papers were also prepared with a procedure similar to that of LBL-TTCS-GO except that the additives were PVA and PMMA respectively, in place of TTCS.

These dry papers then underwent pyrolysis in a tube furnace at 800 °C under argon (Ar) atmosphere for 1h. In order to ascertain the maximum loading of TTCS that could be obtained in a composite paper, additional samples with varied concentrations of TTCS in GO dispersion (40 wt.% along with 70 wt.% TTCS in GO) were prepared. In this study, the samples were labeled as rGO, LBL-SiOC-rGO, PVA-rGO and PMMA-rGO for pristine rGO paper, rGO with 70% of TTCS, rGO with 70% PVA and rGO with 70% PMMA in the total weight of the paper, respectively. The pyrolyzed papers were then cut and used as electrode materials.

2.4 Physical characterization

Scanning electron microscopy (SEM) of the synthesized material was carried out on a Carl Zeiss EVO MA10 system with incident voltage of 5 to 30 kV. High resolution SEM and elemental mapping were performed by use of an FEI company microscope fitted with inbuilt energy dispersive spectroscopy (EDX) silicon drift detector (Oxford Instruments). Material characterization was carried out using an X-ray diffractometer (XRD) operating at room temperature with nickel-filtered Cu K α radiation ($\lambda = 1.5418 \text{ \AA}$). Thermogravimetric analysis was performed using Shimadzu 50 TGA (limited to 800 °C). Samples weighing $\square 2.5 \text{ mg}$ were heated in a platinum pan at a rate of $10 \text{ }^\circ\text{C min}^{-1}$ in air flowing at 20 mL min^{-1} . Fourier Transform Infrared Spectroscopy (FT-IR) spectra were obtained using a Thermo Fisher Nicolet 6700 FT-IR Spectrometer operated in the total attenuated reflectance (ATR) mode.

2.5 Cell assembly and electrochemical measurements

Half-cell batteries were made by punching 14.3 mm diameter out of the paper for use as working electrode. The loading of the active materials was $\sim 2 \text{ mg cm}^{-2}$. A few drops of 1 M Lithium hexafluorophosphate (LiPF $_6$) (Alfa Aesar) dissolved in (1:1 v/v) dimethyl carbonate (Sigma Aldrich): ethylene carbonate (Sigma Aldrich) (ionic

conductivity 10.7 mS cm^{-1}) was used as the electrolyte solution. A 19 mm diameter and 25 μm thick glass separator, soaked in the electrolyte solution was placed between the anode (pyrolyzed paper) and pure Li metal (14.3 mm diameter and 75 μm thick, Alfa Aesar), which acted as a counter electrode. Washer, spring and a top casing were placed on top of the cell to complete the assembly before crimping. This whole procedure was carried out in an Ar-filled glovebox. Electrochemical performance of the battery was tested using a multichannel BT2000 Arbin test unit sweeping between 2.5 V to 10 mV vs Li/Li⁺ at a current density of 50 mA g⁻¹.

Electrochemical properties of the papers as a supercapacitor were studied using a symmetric two electrode configuration on a CHI660E (CH Instruments, Inc.) electrochemical workstation. The devices were assembled by cutting a pair of 0.25 cm² (weighing $\sim 1 \text{ mg}$) area paper from the electrode materials and sandwiching a Whatmann filter paper that has been pretreated in a 6 M potassium hydroxide (KOH, 87.2%, Fisher Scientific) aqueous electrolyte (at room temperature) between them. Both cyclic voltammetry (CV) and galvanostatic charge-discharge (GCD) experiments of the materials were tested in a potential range of 0-0.6 V at various scan rates and current densities, respectively. Electrochemical impedance spectroscopy (EIS) of the materials was analyzed in a frequency range of 1 MHz to 10 mHz at open circuit potential with an alternating voltage of 5 mV amplitude.

3. RESULTS AND DISCUSSION

LBL-SiOC-rGO sandwich composite paper was synthesized by one step pyrolysis of vacuum-filtrated TTCS and GO dispersion which is demonstrated with the help of a schematic (Fig. 1). During pyrolysis, the conversion of TTCS to SiOC as well as reduction of GO to rGO occurs simultaneously. The pyrolyzed papers were more brittle. Yet, structurally strong enough to be used as electrode material. It is believed that liquid TTCS forms a thin layer coating on GO sheets which after pyrolysis, forms a solid ceramic coating on rGO surfaces. To confirm the chemical structure and sandwiched morphology of the composite paper, further characterizations were performed. We also prepared PVA-rGO and PMMA-rGO composite paper (as described in literature⁵⁶) as a standard to study the change in

SEM image of TTCS-GO and LBL-SiOC-rGO free-standing papers are shown in Fig. 2 (a-c) and (d-f), respectively. The high resolution images in Fig. 2(b, e) revealed formation of a layer of TTCS on GO and SiOC on rGO sheets, respectively. Close packing of GO sheets was observed in the cross-sectional SEM images of TTCS-GO paper (Fig. 2c), whereas the LBL-SiOC-rGO papers (Fig. 2f) were more open (each layer seen in the image has multiple sheets of graphene in it). Elemental characterization of the surface by EDX in Fig. 2g confirmed the presence of 11.6 and 12 At.% of Si (1.7 KeV) on the graphene surface in TTCS-GO and LBL-SiOC-rGO composite free-standing papers respectively, along with carbon (0.27 KeV) and oxygen (0.52 KeV).

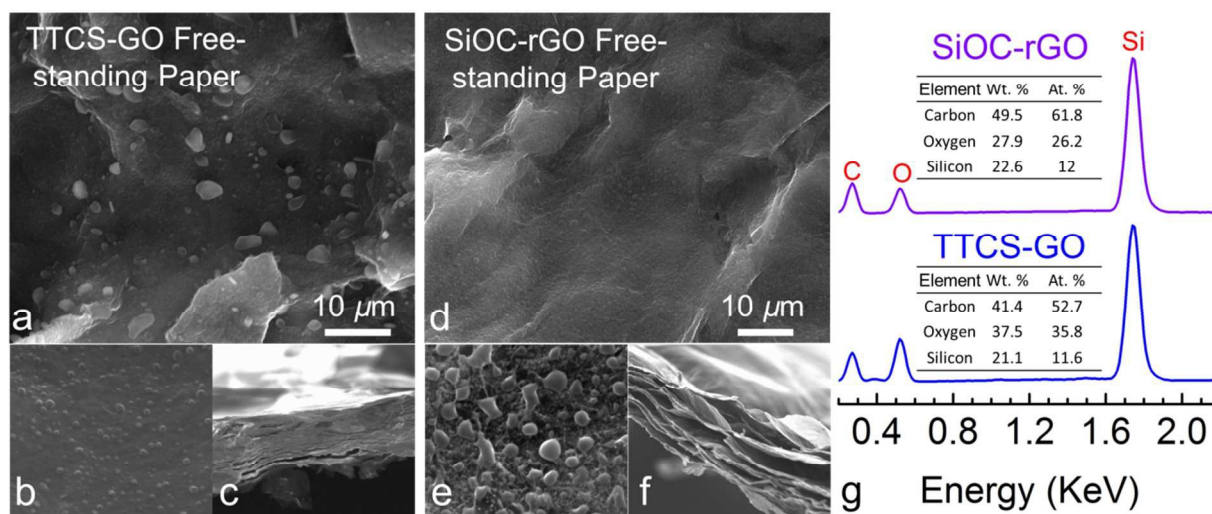


Figure 2. SEM images of free-standing papers (a-c) before and (d-f) after pyrolysis. (b, e) High resolution SEM images showing coating of polymer/ceramic on GO/rGO surface. (c, f) Cross-sectional images of the composite. (g) EDX spectra before and after pyrolysis showing presence of Si in both materials.

XRD and FT-IR spectra of the prepared samples including their TGA curves are presented in Fig. 3(a-d). As shown in Fig. 3a, the XRD spectra of GO and varying percentages of TTCS in GO showed a shift in the GO peak from 10.05° (8.01 \AA) to 9.88° (9 \AA) as the percentage of TTCS in the composite paper increases. The shift in the peak was attributed to an increase in spacing between the individual sheets due to the increased amount of intercalation by TTCS. The insets in Fig. 3a show the cross section of GO and TTCS-GO papers. The total weight of all the papers was 100 mg with respect to the total component (GO and TTCS) weight in the samples.

The thickness of the composite paper decreases with a corresponding increase in the composition of TTCS. This is due to the overall decrease in the GO – an active material that provides structural support for the paper – content of the paper. The comparative XRD spectra of 70%-TTCS-GO with LBL-SiOC-rGO, PVA-rGO, GO and graphite powder are shown in Fig. 3b. GO has a peak at 11.05° which corresponds to a intersheet spacing of 8.01 \AA , while the peaks corresponding to TTCS-GO and PVA-GO papers had shifted to 9.88° (9 \AA) and 5.5° (16.08 \AA) which, as discussed earlier, is due to the intercalation of polymeric precursor in between the sheets of GO.⁵⁶ LBL-SiOC-rGO showed peaks at 24.15° and 26.05° 2θ , which was expected since pyrolysis causes GO to lose intercalated H_2O molecules and $-\text{COOH}$ groups to become rGO.³⁹ In PVA-rGO, the XRD peak was characterized at 26.88° 2θ , which indicates the sheets in rGO were more closely packed as PVA is known to vapourize at $\sim 400^\circ\text{C}$, thus further reducing the graphene interlayer thickness.

Further chemical characterization involving FT-IR was carried out to understand the transformation and formation of functional groups in the samples. The spectra of TTCS-GO composite paper before heat treatment (Fig. 3c) showed typical peaks of intercalated free H_2O molecules, seen at $\sim 3250 \text{ cm}^{-1}$; peaks corresponding to the stretching of $-\text{COOH}$, $-\text{OH}$ and epoxide groups were also observed at ~ 1730 , ~ 1750 and $\sim 1040 \text{ cm}^{-1}$, respectively. The emergence of peaks corresponding to Si-OH (3450 cm^{-1}), Si-H (2100 cm^{-1}), Si- CH_3 (1420 cm^{-1}), and the disappearance of broad peaks corresponding to intercalated free H_2O ($\sim 3250 \text{ cm}^{-1}$) indicates the cleavage of Si- CH_3 and C-H bonds.³⁴ Based on the FT-IR spectra, the following assertions were made: (a) disappearance of H_2O and OH^- peaks at ~ 3250 and 1750 cm^{-1} after heat treatment indicates the removal of water molecules in room temperature to 200°C temperature range, (b) disappearance of $-\text{COOH}$ peak at 1730 cm^{-1} indicates reduction of GO at ~ 200 to 600°C and (c) absence of O-H peak at 1220 cm^{-1} after heat treatment indicates the removal of carboxyl and partial removal of hydroxyl group at $\sim 800^\circ\text{C}$.⁵⁷ For this reason, it can be concluded that reduction of GO to rGO had occurred and the composite paper contains Si both

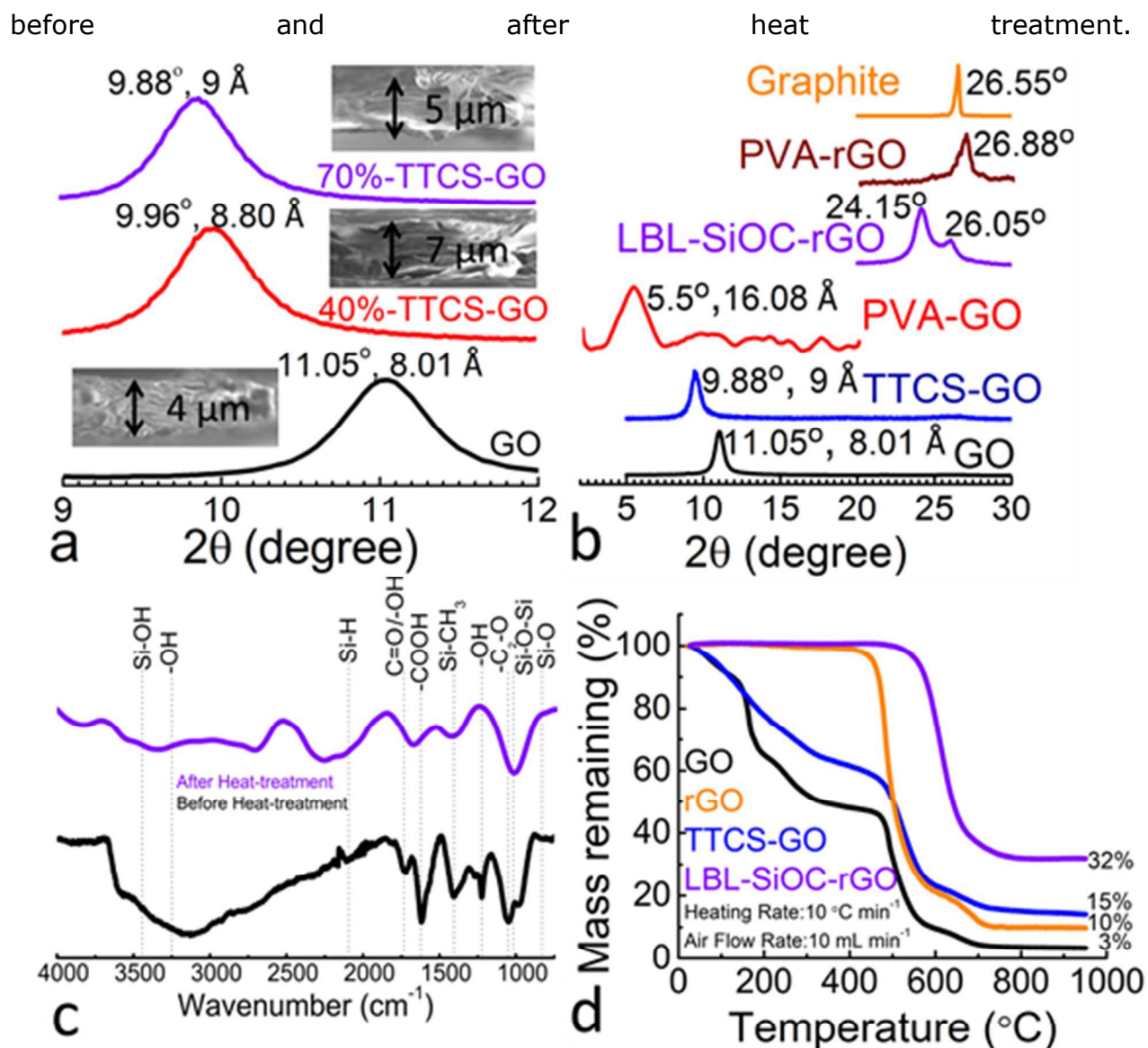


Figure 3. (a) XRD plots of pristine GO and GO paper with variable composition of TTCS (b) Comparative XRD plots of LBL-SiOC-rGO with GO, 70%-TTCS-GO, PVA-GO, PVA-rGO and Graphite (c) FT-IR spectra of TTCS-GO (before heat treatment) and LBL-SiOC-rGO (after heat treatment) (d) TGA plots of GO, rGO, TTCS-GO and LBL-SiOC-rGO.

To further confirm the conversion of GO to rGO and TTCS to SiOC ceramic, TGA was performed (Fig. 3d). It was observed that GO paper had 3% of residual mass with major weight loss at ~ 200 and $\sim 500^\circ\text{C}$ corresponding to the removal of water and burning of carbon material, respectively. The TTCS-GO sample also had a TGA profile similar to GO except that it had 15% mass remaining, possibly due to the

conversion of some part of TTCS present in the composite to SiOC during heating. Meanwhile, rGO had only one weight loss at ~ 500 °C, which was typical of completely reduced GO. LBL-SiOC-rGO specimen had 32% material remaining with most of the weight loss occurring at ~ 650 °C. This suggests 32% of the material in the composite paper was SiOC. Also, SiOC had raised the decomposition temperature of the composite paper by ~ 150 °C, thereby improving the thermal stability of LBL-SiOC-rGO.

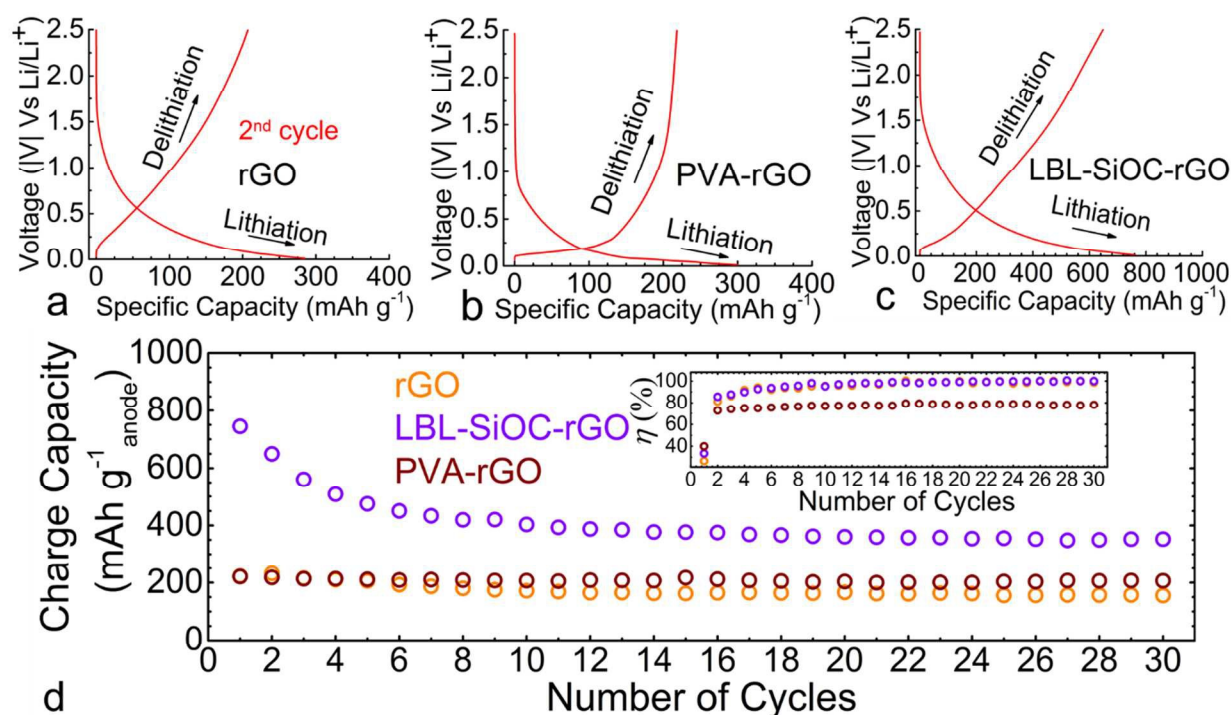


Figure 4. (a-c) 2nd cycle charge/discharge profiles of rGO, PVA-rGO and LBL-SiOC-rGO. (d) Cyclic performance test of rGO, PVA-rGO and LBL-SiOC-rGO (inset shows the corresponding cyclic efficiency comparison).

The composite papers were tested as working electrodes in a LIB half-cell to explore the application of LBL-SiOC-rGO sandwich paper as LIB electrode material. PVA-rGO composite paper was also compared to demonstrate only TTCS polymer-derived SiOC can be a Li-active phase in composite with rGO. Fig. 4(a-c) shows the 2nd charge/discharge profiles of rGO, PVA-rGO and LBL-SiOC-rGO, respectively. rGO and PVA-rGO showed similar 2nd cycle discharge capacities of 280 and 300 mAh g⁻¹ (0.56 and 0.6 mAh cm⁻², respectively) while LBL-SiOC-rGO clearly had much higher

capacity of 780 mAh g^{-1} (1.56 mAh cm^{-2}). Fig. 4d shows the charge capacities and Columbic efficiency of rGO, PVA-rGO and LBL-SiOC-rGO anodes cycled at a constant current density of 50 mA g^{-1} for 30 cycles. For rGO, a stable charge capacity at $\sim 190 \text{ mAh g}^{-1}$ (0.38 mAh cm^{-2}) in the 30th cycle was observed. All electrodes showed relatively high first cycle loss (Fig. 4d). Previous studies have shown that the observed low initial Columbic efficiency of the electrodes is majorly due to the following reasons: decomposition of the electrolyte resulting in the formation of a passive solid-electrolyte interface (SEI), side reaction of Li with the electrolyte's decomposed compound and any moisture contamination, formation of irreversible phases with SiOC, and the contributing first cycle loss due to presence of rGO.^{6,50,58} In the LBL-SiOC-rGO composite, after an initial drop in the capacity, the charge capacity remained constant at 400 mAh g^{-1} (0.8 mAh cm^{-2}) for 30 cycles. In comparison, the PVA-rGO polymer composites showed a Coulombic efficiency of $\sim 70\%$, which is lesser than that of rGO ($\sim 80\%$). It is believed that the superior electrochemical performance of LBL-SiOC-rGO as a battery electrode could be due to formation of a stable solid ceramic coating on the surface of rGO as a result of the transformation of liquid polymeric TTCS to ceramic SiOC unlike PVA. The SiOC ceramic coating on rGO acts as a Li-active phase that contains Si and C dangling bonds (Li intercalation sites) and amorphous carbon linkages (which enhances nano-level electrical conductivity).⁶

The electrochemical properties of the LBL-SiOC-rGO as a supercapacitor electrode was investigated and compared with PVA-rGO and PMMA-rGO composite. The supercapacitor electrochemical test was carried out using a two-electrode setup. Preliminary studies involving CV and EIS were carried out to determine the best performing electrode material (Fig. 5(a-b)). The CV curves of LBL-SiOC-rGO, PVA-rGO and PMMA-rGO at a scan rate of 200 mV s^{-1} are presented in Fig. 5a. The electrode materials display a quasi-rectangular curve, suggesting the presence of electrochemical charge transfer processes. However, the integral area of PVA-rGO and PMMA-rGO is too small compared to LBL-SiOC-rGO. For this reason, it is evidence that LBL-SiOC-rGO demonstrates the superior capacitive behavior. Moreover, LBL-SiOC-rGO displays a broad reduction peak at a potential of $\sim 0.38 \text{ V}$. This is

synonymous to a pseudocapacitive material with a dominant Faradaic process possibly due to the presence of oxygen-containing molecules in the material.⁵⁹

Furthermore, the Faradaic resistance of the electrode materials were investigated using the EIS (Fig. 5b). The left intercept of the semicircle with the real axis (Z') is a measure of dominant resistive behavior due to the interface between the electrolyte, electrode and current collector (commonly referred to interfacial resistance). From the inset of the Nyquist plots shown (Fig. 5b, inset i), only LBL-SiOC-rGO electrode shows an almost perfect semicircle. Compared to other electrode materials, LBL-SiOC-rGO has the least interfacial resistance corresponding to 0.47Ω (as shown in Fig. 5b, inset ii). The right intercept of the semicircle with Z' represents the internal resistance of an electrode material. When the curves of the electrodes at the lower frequency region are imaginarily fitted into a semicircle, LBL-SiOC-rGO has the least internal resistance corresponding to $\sim 4.86 \Omega$, which is believed to be far lesser than the internal resistance of PMMA-rGO and PVA-rGO electrode; hence, the LBL-SiOC-rGO in the electrolyte is kinetically fast. For this reason, the electrical conductivity of LBL-SiOC-rGO is expected to be the highest due to its lower particle parking (as shown in the SEM images in Fig. 2(d-f)) and lower diffusion path length of ions; hence, a larger capacitance. This result corroborates the CV shown in Fig. 5a. A long steep slope in the low frequency region indicates a dominant capacitive behavior due to the efficient diffusion of ions onto the pores of the electrode.⁶⁰ As shown Fig. 5b, LBL-SiOC-rGO has the steepest slope with an appreciable low frequency tail. As such, it is obvious that LBL-SiOC-rGO has the highest capacitance among the electrode materials being tested.

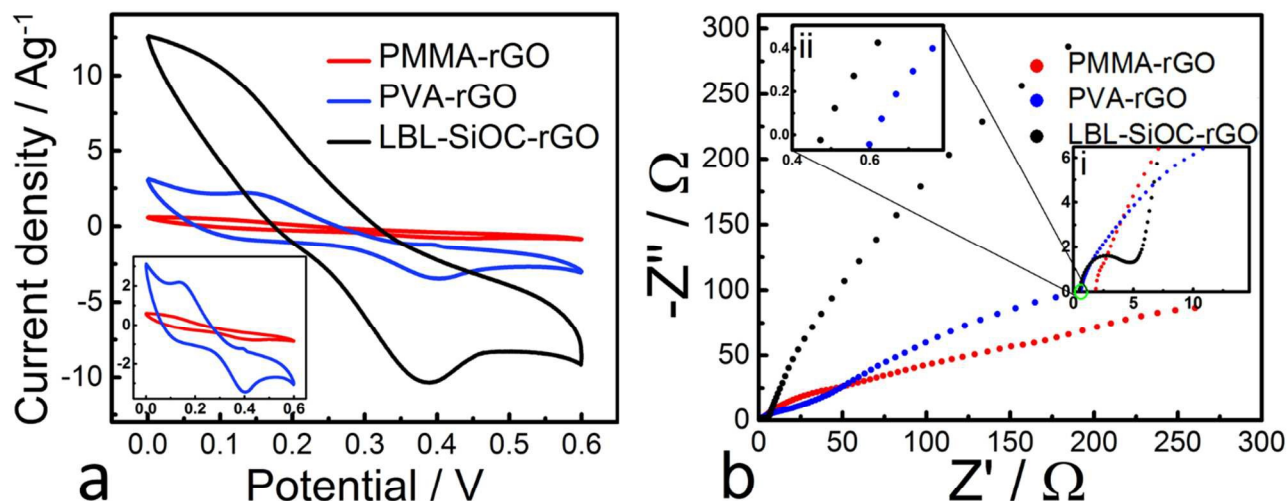


Figure 5. (a) Cyclic voltammogram of PMMA-rGO, PVA-rGO and LBL-SiOC-rGO at 200 mV s^{-1} (inset shows expanded CV of PVA-rGO and PMMA-rGO) (b) Nyquist plots for PMMA-rGO, PVA-rGO and LBL-SiOC-rGO electrodes (inset shows expanded plots at high frequency region).

Since LBL-SiOC-rGO is the best performing electrode (based on preliminary experiments), further CV and GCD including cyclic stability test were performed to study its capacitive behavior. CVs, GCDs and cyclic stability plots of LBL-SiOC-rGO symmetric two-electrode setup recorded over a potential window of 0-0.6V at various scan rates and current densities in 6.0 M KOH electrolyte are shown in Fig. 6(a-c) respectively.

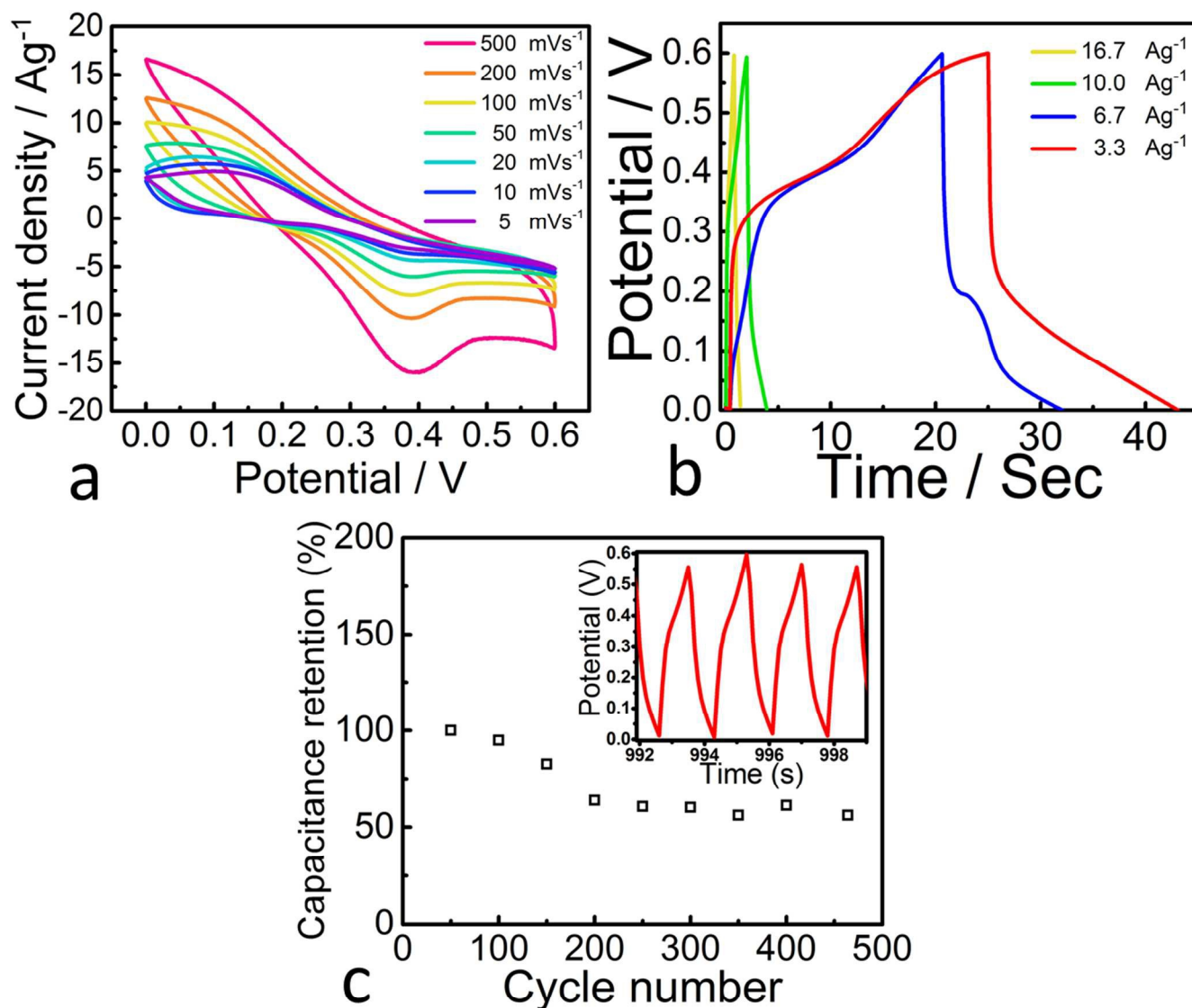


Figure 6. (a) Cyclic voltammograms of LBL-SiOC-rGO at different scan rates, (b) Galvanostatic charge-discharge curves of LBL-SiOC-rGO at various current densities, (c) Capacitance retention plot of LBL-SiOC-rGO as a function of cycle number at a current density of 6.7 A g⁻¹ (inset shows representative last cycle charge-discharge curve).

The CV curves of LBL-SiOC-rGO shows quasi-rectangular curves with redox peaks around 0.4 and 0.1 V which is suggestive of dominant Faradaic processes.⁶¹ From the GCD measurements shown in Fig. 6b, the LBL-SiOC-rGO charge and discharge curves shows a distorted triangle with a discharge curve characterized by a slow discharge occurring after a potential of 0.2 V. This nonlinear discharge process is

typical of pseudocapacitive materials. Furthermore, it can be inferred that the LBL-SiOC-rGO electrode material is favorably able to accommodate diffusion of the electrolyte's ions onto its surface.^{61,62} The specific capacitance of LBL-SiOC-rGO was calculated from the slope of its GCD curve using the expression below:

$$C_s = 2I\Delta t / m\Delta V \quad (1)$$

Where C_s , I , Δt , m and ΔV is the specific capacitance ($F g^{-1}$), applied current (A), average mass of the electrodes (g), discharge time (sec) and corresponding potential window (V, excluding iR drop during the discharge process), respectively. LBL-SiOC-rGO had a specific capacitance of $586.66 F g^{-1}$ at a current density of $3.3 A g^{-1}$ which decreases to $70.18 F g^{-1}$ at higher current density ($16.7 A g^{-1}$). When evaluating the cyclic stability of the LBL-SiOC-rGO electrode at a current density of $6.7 A g^{-1}$, an initial capacitance of $75.72 F g^{-1}$ (after the 10th cycle) with a capacitance retention of 56.13% (corresponding to $37.35 F g^{-1}$) after 464 cycles was obtained. A comparison of the obtained specific capacitance of LBL-SiOC-rGO in relation to previously reported PDCs is presented in Table 1.

Table 1 Comparison of the specific capacitance of some composite electrodes in relation to present work

Materials	Electrolyte	Voltage window (V)	Current density/ Scan rate	Specific Capacitance ($F g^{-1}$)	Ref.
CNT/Graphite	3M LiNO ₃	-0.5 to 0.7	20 mV s ⁻¹	25	63
TC	1 M TEATFB in 50-50 PC-DMC	0 to 2	0.074 A g ⁻¹	33.2	64
PGM-Fe-800	1M Et ₄ NBF ₄ in AC	0 to 2	0.7 A g ⁻¹	31	65
SWCNT/TBAP	0.2 M DmFc, 1 M TBAP/THF	0 to 2.1	1.0 A g ⁻¹	61.3	66
LBL-SiOC-rGO	6 M KOH	0 to 0.6	6.7 A g ⁻¹	75.72	Present work

Although the specific capacitance of the LBL-SiOC-rGO electrode is lesser than that of some similar PDCs that have been reported in the literature,^{52,67,68} the specific capacitance is more realistic because it is a free-standing electrode, which implies it is additive-free (e.g. binders and conducting materials) and does not require the

use of current collectors which obscure its true capacitance value. LBL-SiOC-rGO displays some charge storage capability as an electrode material for supercapacitor possibly due to the synergistic effect between SiOC and rGO. In this configuration, we believe the disordered carbon in SiOC is responsible for its charge storage capability. However, rGO plays a dominant role in the charge storage process of the composite. Overall, LBL-SiOC-rGO is more promising as a battery electrode.⁶

4. CONCLUSION

In summary, we have demonstrated the single step synthesis of a free-standing sandwich paper from TTCS and GO consisting of a layer-by-layer self-assembled rGO sheets with SiOC ceramic in the interlayer galleries. The intercalation of rGO sheets by SiOC, formation of a ceramic coating on the rGO sheets, and improved performance was established by comparing other composite electrodes prepared from non-silicon based precursors (PVA and PMMA). The resulting structure of LBL SiOC-rGO provided a solid contact between the electrically conducting rGO sheets and Li intercalating SiOC ceramic. As a result, high reversible capacity of 750 mAh g⁻¹ was achieved when used as an electrode for LIB, while a specific capacitance of 75.72 F g⁻¹ and a capacitance retention of 56.13% after 464 cycles were obtained when tested as an electrode material in a symmetric two electrode supercapacitor.

Although promising in terms of energy density, design simplicity (no inactive components) and costs, there are some new challenges that must be addressed before the LBL-SiOC-rGO electrodes could be commercialized, these include: (a) small lateral dimensions of the paper electrode that are limited by the vacuum filtration setup (a diameter of ~15 cm diameter) and (b) the brittle nature of the pyrolyzed paper which may limit its long term cyclability as a highly flexible and bendable energy storage material.

ACKNOWLEDGEMENTS

A portion of this research is based on work supported by the National Science Foundation-grant No. 1335862 and 1454151 to G. Singh.

REFERENCES

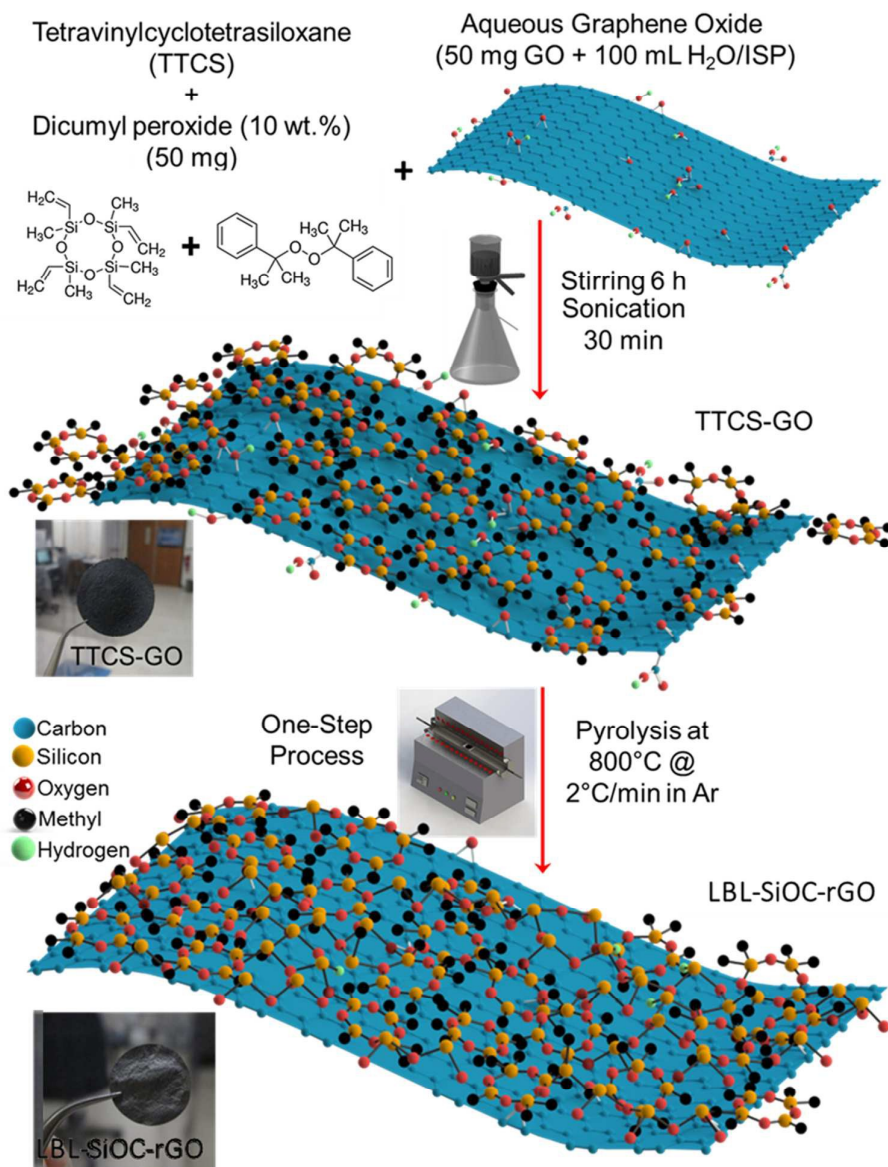
- 1 J. M. Tarascon and M. Armand, *Nature*, 2001, **414**, 359.
- 2 B. Dunn, H. Kamath and J. M. Tarascon, *Science*, 2011, **334**, 928.
- 3 X. W. Lou, L. A. Archer and Z. Yang, *Adv. Mater.*, 2008, **20**, 3987.
- 4 Y. G. Guo, J. S. Hu and L. J. Wan, *Adv. Mater.*, 2008, **20**, 2878.
- 5 P. G. Bruce, B. Scrosati and J. M. Tarascon, *Angew. Chem., Int. Ed.*, 2008, **47**, 2930.
- 6 L. David, R. Bhandavat, U. Barrera and G. Singh, *Nat. Commun.*, 2016, **7**, 10998.
- 7 Z. S. Wu, W. Ren, L. Wen, L. Gao, J. Zhao, Z. Chen, G. Zhou, F. Li and H. M. Cheng, *ACS Nano*, 2010, **4**, 3187.
- 8 W. Zhou, J. Zhu, C. Cheng, J. Liu, H. Yang, C. Cong, C. Guan, X. Jia, H. J. Fan, Q. Yan, C. M. Li and T. Yu, *Energy Environ. Sci.*, 2011, **4**, 4954.
- 9 S. M. Paek, E. Yoo and I. Honma, *Nano Lett.*, 2009, **9**, 72.
- 10 L. David and G. Singh, *J. Phys. Chem. C*, 2014, **118**, 28401.
- 11 W. M. Zhang, X. L. Wu, J. S. Hu, Y. G. Guo and L. J. Wan, *Adv. Funct. Mater.*, 2008, **18**, 3941.
- 12 Y. Chen, Y. Zhang, D. Geng, R. Li, H. Hong, J. Chen and X. Sun, *Carbon*, 2011, **49**, 4434.
- 13 R. Bhandavat, L. David and G. Singh, *J. Phys. Chem. Lett.*, 2012, **3**, 1523.
- 14 H. Guan, X. Wang, S. Chen, Y. Bando and D. Golberg, *Chem. Commun.*, 2011, **47**, 12098.
- 15 H. Wang, L. F. Cui, Y. Yang, H. Sanchez Casalongue, J. T. Robinson, Y. Liang,

- Y. Cui and H. Dai, *J. Am. Chem. Soc.*, 2010, **132**, 13978.
- 16 S. Yang, X. Feng, S. Ivanovici and K. Müllen, *Angew. Chem. Int. Ed.*, 2010, **49**, 8408.
- 17 L. Ji, H. Zheng, A. Ismach, Z. Tan, S. Xun, E. Lin, V. Battaglia, V. Srinivasan and Y. Zhang, *Nano Energy*, 2012, **1**, 164.
- 18 A. Kumar, A. L. M. Reddy, A. Mukherjee, M. Dubey, X. Zhan, N. Singh, L. Ci, W. E. Billups, J. Nagurny, G. Mital and P. M. Ajayan, *ACS Nano*, 2011, **5**, 4345.
- 19 X. Li, D. Geng, Y. Zhang, X. Meng, R. Li and X. Sun, *Electrochem. Commun.*, 2011, **13**, 822.
- 20 P. Ge and M. Fouletier, *Solid State Ionics*, 1988, **28**, 1172.
- 21 H. Zhu, Z. Jia, Y. Chen, N. Weadock, J. Wan, O. Vaaland, X. Han, T. Li and L. Hu, *Nano Lett.*, 2013, **13**, 3093.
- 22 L. David, R. Bhandavat and G. Singh, *ACS Nano*, 2014, **8**, 1759.
- 23 D. Wang, R. Kou, D. Choi, Z. Yang, Z. Nie, J. Li, L. V. Saraf, D. Hu, J. Zhang, G. L. Graff, J. Liu, M. A. Pope and I. A. Aksay, *ACS Nano*, 2010, **4**, 1587.
- 24 L. David, K. M. Shareef, M. A. Abass and G. Singh, *RSC Adv.*, 2016, **6**, 53894.
- 25 Z. Chen, M. Zhou, Y. Cao, X. Ai, H. Yang and J. Liu, *Adv. Energy Mater.*, 2012, **2**, 95.
- 26 G. Zhou, D. W. Wang, F. Li, L. Zhang, N. Li, Z. S. Wu, L. Wen, G. Q. Lu and H. M. Cheng, *Chem. Mater.*, 2010, **22**, 5306.
- 27 L. Ji, Z. Tan, T. R. Kuykendall, S. Aloni, S. Xun, E. Lin, V. Battaglia and Y. Zhang, *Phys. Chem. Chem. Phys.*, 2011, **13**, 7170.
- 28 D. Wang, D. Choi, J. Li, Z. Yang, Z. Nie, R. Kou, D. Hu, C. Wang, L. V. Saraf,

- J. Zhang, I. A. Aksay and J. Liu, *ACS Nano*, 2009, **3**, 907.
- 29 J. Xiao, X. Wang, X. Q. Yang, S. Xun, G. Liu, P. K. Koech, J. Liu and J. P. Lemmon, *Adv. Funct. Mater.*, 2011, **21**, 2840.
- 30 J. K. Lee, K. B. Smith, C. M. Hayner and H. H. Kung, *Chem. Commun.*, 2010, **46**, 2025.
- 31 Y. Wang, H. Li, P. He, E. Hosono and H. Zhou, *Nanoscale*, 2010, **2**, 1294.
- 32 L. Ji, Z. Tan, T. Kuykendall, E. J. An, Y. Fu, V. Battaglia and Y. Zhang, *Energy Environ. Sci.*, 2011, **4**, 3611.
- 33 V. S. Pradeep, M. Graczyk-Zajac, R. Riedel and G. D. Soraru, *Electrochim. Acta*, 2014, **119**, 78.
- 34 R. Bhandavat and G. Singh, *J. Phys. Chem. C*, 2013, **117**, 11899.
- 35 R. Bhandavat and G. Singh, *ACS Appl. Mater. Interfaces*, 2012, **4**, 5092.
- 36 R. Kolb, C. Fasel, V. Liebau-Kunzmann and R. Riedel, *J. Eur. Ceram. Soc.*, 2006, **26**, 3903.
- 37 M. Graczyk-Zajac, C. Fasel and R. Riedel, *J. Power Sources*, 2011, **196**, 6412.
- 38 Y. Feng, N. Feng, Y. Wei and Y. Bai, *J. Mater. Chem. A*, 2014, **2**, 4168.
- 39 M. Graczyk-Zajac, G. Mera, J. Kaspar and R. Riedel, *J. Eur. Ceram. Soc.*, 2010, **30**, 3235.
- 40 J. Kaspar, G. Mera, A. P. Nowak, M. Graczyk-Zajac and R. Riedel, *Electrochim. Acta*, 2010, **56**, 174.
- 41 Y. Feng, *Electrochim. Acta*, 2010, **55**, 5860.
- 42 D. Ahn and R. Raj, *J. Power Sources*, 2010, **195**, 3900.
- 43 A. Saha, R. Raj and D. L. Williamson, *J. Am. Ceram. Soc.*, 2006, **89**, 2188.

- 44 H. Fukui, N. Nakata, K. Dokko, B. Takemura, H. Ohsuka, T. Hino and K. Kanamura, *ACS Appl. Mater. Interfaces*, 2011, **3**, 2318.
- 45 J. Shen, D. Ahn and R. Raj, *J. Power Sources*, 2011, **196**, 2875.
- 46 H. Fukui, H. Ohsuka, T. Hino and K. Kanamura, *J. Electrochem. Soc.*, 2011, **158**, A550.
- 47 V. Liebau-Kunzmann, C. Fasel, R. Kolb and R. Riedel, *J. Eur. Ceram. Soc.*, 2006, **26**, 3897.
- 48 D. Su, Y. L. Li, Y. Feng and J. Jin, *J. Am. Ceram. Soc.*, 2009, **92**, 2962.
- 49 H. Tamai, H. Sugahara and H. Yasuda, *J. Mater. Sci. Lett.*, 2000, **19**, 53.
- 50 H. Fukui, H. Ohsuka, T. Hino and K. Kanamura, *ACS Appl. Mater. Interfaces*, 2010, **2**, 999.
- 51 M. Wang, Y. Xia, X. Wang, Y. Xiao, R. Liu, Q. Wu, B. Qiu, E. Metwalli, S. Xia, Y. Yao, G. Chen, Y. Liu, Z. Liu, J. Q. Meng, Z. Yang, L. D. Sun, C. H. Yan, P. Müller-Buschbaum, J. Pan and Y. J. Cheng, *ACS Appl. Mater. Interfaces*, 2016, **8**, 13982.
- 52 A. Tolosa, B. Krüner, N. Jäckel, M. Aslan, C. Vakifahmetoglu and V. Presser, *J. Power Sources*, 2016, **313**, 178.
- 53 Y. J. Lee, J. Y. Ryu, K. C. Roh, S. R. Kim, W. T. Kwon, D-G. Shin and Y. Kim, *J. Korean Ceram. Soc.*, 2013, **50**, 480.
- 54 W. S. Hummers and R. E. Offeman, *J. Am. Chem. Soc.*, 1958, **80**, 1339.
- 55 D. C. Marcano, D. V. Kosynkin, J. M. Berlin, A. Sinitskii, Z. Sun, A. Slesarev, L. B. Alemany, W. Lu and J. M. Tour, *ACS Nano*, 2010, **4**, 4806.
- 56 K. W. Putz, O. C. Compton, M. J. Palmeri, S. T. Nguyen and L. C. Brinson, *Adv. Funct. Mater.*, 2010, **20**, 3322.

- 57 D. Li, M. B. Müller, S. Gilje, R. B. Kaner and G. G. Wallace, *Nat. Nanotechnol.*, 2008, **3**, 101.
- 58 V. Agubra and J. Fergus, *Materials*, 2013, **6**, 1310.
- 59 Y. Zhang, X. Li, J. Huang, W. Xing and Z. Yan, *Nanoscale Res. Lett.*, 2016, **11**, 163.
- 60 H. Hu, Z. Hu, X. Ren, Y. Yang, R. Qiang, N. An and H. Wu, *Chinese J. Chem.*, 2015, **33**, 199.
- 61 M. S. Kolathodi, M. Palei and T. S. Natarajan, *J. Mater. Chem. A*, 2015, **3**, 7513.
- 62 M. S. Kolathodi and T. S. Natarajan, *Scr. Mater.*, 2015, **101**, 84.
- 63 P. Bondavalli, C. Delfaure, P. Legagneux and D. Pribat, *J. Electrochem. Soc.*, 2013, **160**, A601.
- 64 Y. Zhou, S. L. Candelaria, Q. Liu, E. Uchaker and G. Cao, *Nano Energy*, 2015, **12**, 567.
- 65 M. Sevilla and A. B. Fuertes, *Carbon*, 2013, **56**, 155.
- 66 J. Park, B. Kim, Y. E. Yoo, H. Chung and W. Kim, *ACS Appl. Mater. Interfaces*, 2014, **6**, 19499.
- 67 A. Meier, M. Weinberger, K. Pinkert, M. Oschatz, S. Paasch, L. Giebeler, H. Althues, E. Brunner, J. Eckert and S. Kaskel, *Microporous Mesoporous Mater.*, 2014, **188**, 140.
- 68 L. Duan, Q. Ma, L. Mei and Z. Chen, *Microporous Mesoporous Mater.*, 2015, **202**, 97.



Graphical Abstract